



Modelling of Reinforced Concrete Columns with GFRP Rebar

Robert K. Dowell¹, Francesca Ferretti², Claudio Mazzotti², and Gloria Faraone¹(✉)

¹ San Diego State University, San Diego, CA 92182, USA
gfaraone@sdsu.edu

² DICAM Department, University of Bologna, Viale Risorgimento 2, 40136 Bologna, Italy

Abstract. Concrete structures reinforced with glass fiber-reinforced polymer (GFRP) bars are becoming increasingly popular, particularly in harsh environments where traditional steel reinforcement may be susceptible to corrosion and accelerated damage. GFRPs are a possible solution in such climates, since they are not affected by corrosion and have high tensile strength. The assessment of GFRP-reinforced concrete structural response to lateral loads, however, is still in a preliminary stage. Despite the need for robust numerical tools to estimate the lateral displacement and ductility capacities of GFRP-reinforced structural elements, current numerical modeling is limited by the lack of reliable full-range axial stress vs strain models, or by insufficient description of the behavior of GFRP-confined concrete. This paper aims at providing a contribution to the analytical modeling of the response to lateral loads of GFRP-reinforced concrete elements. Four scaled RC bridge columns have been designed (with the same nominal strength) and built for testing to failure under simulated earthquake loading at San Diego State University (SDSU), with various combinations of steel and GFRP bars, from all-steel to all-GFRP. In this work, GFRP reinforcement is considered for both the primary vertical and transverse reinforcements. Prediction analyses of the four different columns to failure are discussed in this paper, including a technique of incremental confinement which is crucial for concrete confined by GFRP.

Keywords: Cyclic loading · Glass fiber-reinforced polymer (GFRP) rebar · Reinforced concrete · Confined concrete · Hoop strain · Incremental confinement

1 Introduction

The use of glass fiber-reinforced polymer (GFRP) bars as a construction material in reinforced concrete (RC) has increased in recent years, mainly due to the low corrosion susceptibility and high tensile strength of this material. Among RC structural elements, bridge columns may be significantly exposed to severe environmental conditions, hence these elements would particularly benefit from the use of GFRPs as longitudinal and/or transverse reinforcement. RC bridge columns are typically designed and built using steel for both the primary vertical reinforcement and transverse reinforcement. Vertical reinforcement is designed for bending and axial forces, while transverse reinforcement, at a given spacing or pitch up the column height, provides added shear capacity to

the concrete, prevents buckling of the primary vertical rebar and ensures confinement to the core concrete [1]. For circular columns, transverse reinforcement is given in the form of a continuous spiral, or multiple individual hoops for larger reinforcing bars, with spacing defined up the column. Confinement provided to the core concrete by the closely-spaced transverse reinforcement significantly increases the compressive strain capacity of the confined concrete at the extreme edge of the section in bending, resulting in larger plastic curvature and rotation capacities at the critical section at the column ends where the moment is maximum [1]. This gives a bridge structure the needed displacement capacity to resist displacement demands from a large earthquake [2]. Given these conditions, GFRPs may strategically substitute for steel reinforcement, as other studies have shown [3–7]. In this paper, analytical modeling is developed to predict the performance of varied GFRP-reinforced bridge columns under lateral loads.

2 Test Specimens

Four circular RC bridge columns have been designed and built at San Diego State University (SDSU) with the same overall dimensions but with different combinations of steel rebar and GFRP, as shown in Figs. 1 and 2. The columns have a diameter of 1'–6" (0.457 m) and height of 5' (1.52 m) from top-of-footing to the center of the load stub where lateral loading will be applied cyclically in deformation control, simulating earthquake demands. They will be fixed at the base and free to rotate at the top where the lateral load is applied, acting as a cantilever with constant shear and linearly increasing moment from zero at the top to the maximum moment at the column base where the plastic hinge develops. An axial compression load of 66 kips (294 kN) will be provided to the top of the columns before lateral loads are applied, representing the scaled weight of a prototype bridge structure with about 5% axial load ratio. Column dimensions came from scaling the full-scale prototype bridge that has columns which are fixed at both ends, i.e., at their footings and superstructure, by modeling only half the column height, from the base to the point-of-inflection where the moment is zero. Thus, a cantilever column correctly captures the lower half of the fixed-fixed bridge column of the prototype bridge structure, which has a 6' (1.83 m) diameter and height of 36' (11.0 m). The columns are 1:4 scale. All four columns were designed with the same nominal strength, resulting in different expected displacement capacities since steel reinforcing bar is ductile and GFRP reinforcing bar is brittle.

The purpose of these experimental tests is to determine how well GFRP rebar works in place of standard steel reinforcement, for both the primary vertical and transverse reinforcements (Fig. 1). Strategic configurations can be developed to take advantage of both materials in critical and non-critical sections, e.g., a region of plasticity versus a linear-elastic region. For example, Column 2 has steel vertical bars and GFRP transverse spiral at close spacing in the plastic hinge zone, with wider spacing above this, and Column 3 has GFRP vertical and transverse reinforcement, with steel starter bars that carry the moment (and local deformations) from the column to the footing. Besides these hybrid solutions, configurations with all-steel (Column 1) and all-GFRP (Column 4) rebar are included. Column 1 has 17 #5 vertical steel rebar and #3 transverse steel spiral at 2.75" (6.99 cm) spacing, Column 2 has 17 #5 vertical steel rebar and #3 transverse GFRP

spiral at 0.87" (2.21 cm) spacing in the plastic hinge zone, Column 3 has 17 #5 vertical steel starter bars (and 19 #5 vertical GFRP rebar that start above the column/footing interface) and #3 transverse GFRP spiral at 0.87" (2.21 cm) in the plastic hinge zone, and Column 4 has 19 #5 vertical GFRP rebar and #3 transverse GFRP spiral at 0.87" (2.21 cm) in the plastic hinge zone. Cover to the transverse reinforcement for all four columns is 0.5" (1.27 cm).

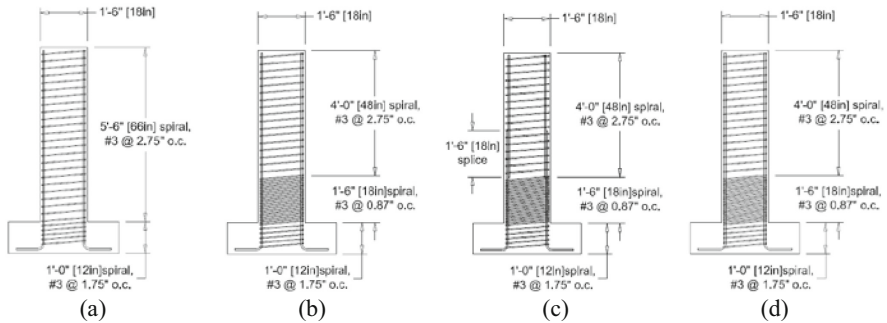


Fig. 1. Columns' details (a) Column 1: vertical and transverse steel rebar; (b) Column 2: vertical steel rebar and GFRP transverse rebar; (c) Column 3: vertical and transverse GFRP rebar/starter steel rebar; and (d) Column 4: vertical and transverse GFRP rebar. (1 in. = 2.54 cm)

This gives a vertical steel rebar ratio for Columns 1, 2 and 3 of 2.07% and vertical GFRP rebar ratio of 2.29% for Column 4. The transverse rebar ratios are 0.962% and 3.04% for steel Column 1 and for GFRP Columns 2, 3 and 4, respectively. Vertical rebar is distributed evenly around the column cross-section. GFRP rebar has deformations that are consistent with steel rebar, and therefore bond between rebar and concrete, and strain-penetration of vertical rebar from the column into the footing is treated the same for GFRP as for steel. Prediction analyses shown below indicate that all four columns fail due to hoop strains exceeding their capacities for both the steel and GFRP transverse reinforcing bars.



Fig. 2. Rebar cages and finished columns.

To understand the different responses to lateral loads of these various configurations, this paper focuses on prediction analyses for all four columns and analytically determines how well GFRP compares to steel reinforcement. To properly account for the confinement provided by transverse GFRP rebar, compared to what is typically done for steel, an incremental form of the Mander model for confined concrete [8] has been implemented within the program ANDRIANNA [9], which was specifically developed for RC columns. Although a constant confinement model may be used for a column that has steel transverse reinforcement with satisfactory results (since the transverse steel yields early in the analysis), one of the advantages of the incremental confinement approach is that hoop strains are monitored throughout the analysis, which is not possible in the Mander model [8]. As an example, multiple RC bridge structures had welded steel hoop confinement with limited strain capacity due to inferior welds, requiring the incremental confinement approach to assess the reduced bridge displacement capacities [10, 11]. In this paper, all four columns are analyzed with the incremental confinement approach. Uniaxial tensile tests were conducted to failure for the primary vertical steel and GFRP reinforcing bar, and concrete cylinders were tested in compression, providing measured material properties used in all analyses herein.

3 Material Coupon Tests

Results from three steel coupon tests of the primary vertical bars are given in Fig. 3a, as well as the idealized response used in the column analyses. The average yield stress along the yield plateau for each reinforcing bar was found by taking the average of all the measured stress data between strains of 0.003 and 0.01, with the lower and upper bounds chosen to make sure that the stress-strain responses were on the yield plateau for all three coupons. The idealized average yield stress is 72.5 ksi (500 MPa), the average ultimate stress is 98.1 ksi (676 MPa), and average ultimate strain is 0.122. The standard modulus of elasticity E value of 29,000 ksi (200,000 MPa) for steel was used since this was within the accuracy of the measurements, giving the idealized yield strain of $72.5/29,000 = 0.0025$. The average unconfined concrete strength from three cylinder tests was 5.60 ksi (38.6 MPa).

Given the yield stress (σ_y) and strain (ϵ_y), ultimate stress (σ_u) and strain (ϵ_u), as well as strain at first hardening (ϵ_h), which represents the end of the yield plateau and onset of strain-hardening, the measured strain-hardening portion of the curve is best represented by Eq. 1:

$$\sigma = \sigma_y + a(\epsilon - \epsilon_h) + b(\epsilon - \epsilon_h)^2 + c(\epsilon - \epsilon_h)^3 \quad (1)$$

Boundary conditions of ultimate stress at ultimate strain, zero slope at ultimate stress, and initial slope of the strain-hardening portion of the curve (E_m), allows the constants for Eq. 1 to be found as:

$$a = E_m = 710; \quad b = (3\sigma_0 - 2E_m \epsilon_0)/\epsilon_0^2 = -6564; \quad c = -(E_m + 2b \epsilon_0)/3\epsilon_0^2 = 20227 \quad (2)$$

with

$$\sigma_0 = (\sigma_u - \sigma_y) = (98.1 - 72.5) = 25.6 \text{ ksi}; \quad \epsilon_0 = (\epsilon_u - \epsilon_y) = (0.12 - 0.012) = 0.108. \quad (3)$$

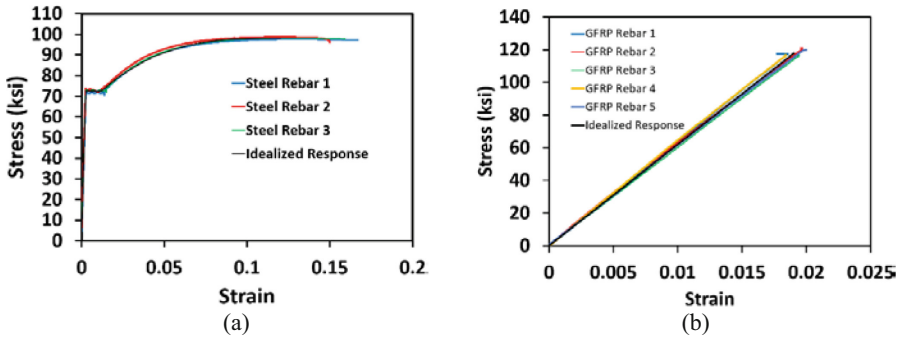


Fig. 3. Stress-strain results of (a) steel rebar and (b) GFRP rebar and idealized response idealized response (1 ksi = 6.895 MPa)

Five coupon tests were conducted for the primary vertical GFRP reinforcing bar, as shown in Fig. 3b, along with the idealized response. Results to onset of failure are shown for all five tests, as indicated by the sudden offset from the straight line. The slope of the idealized stress-strain response was found from the average of the five coupon slopes, taken at 100 ksi (6891 MPa) stress, while the idealized ultimate stress was determined from the average of the five coupon stresses where onset of failure happened. This produced a slope, or modulus of elasticity, of the stress-strain diagram for the GFRP of 6200 ksi (42,750 MPa) and ultimate stress of 118 ksi (814 MPa), which give the ultimate strain of 0.0190 for the GFRP reinforcing bar. Comparing the idealized stress-strain responses of the steel and GFRP rebar (Fig. 3) is very interesting, with GFRP having a much softer initial slope than the steel modulus of elasticity of 29000 ksi (200,000 MPa) – by a factor of almost five –, crossing the steel stress-strain curve close to the end of the yield plateau (start of strain-hardening). But then the GFRP continues linearly to failure, with larger ultimate stress than the steel, and at a much smaller strain.

4 Prediction Analysis Results

The incremental confinement approach allows the concrete to expand into the linear or nonlinear material wrapped around it, causing a changing hoop tension that confines the concrete. For steel confinement, the transverse bars yield early, and then apply constant confinement for the duration of the analysis. This is the reason that the Mander model for confined concrete [8] works so well for RC bridge columns that are reinforced with steel; in this approach, the stress-strain response of confined concrete is determined before the lateral column analysis. However, GFRP exhibits a linear-elastic behavior until failure and, therefore, as the vertical compression strains increase with bending, the concrete expands out into the GFRP transverse reinforcement, with hoop strains and stresses continuing to increase, resulting in changing confining stresses throughout the loading. For this case, the assumption of constant confining stress is not realistic, requiring an incremental confinement approach, as used for all four columns herein.

Based on an energy balance method, the current expansion rate for each slice of the critical cross-section is found [10, 11]. This represents a changing, and increasing,

Poisson’s ratio from the linear-elastic value at the start of the analysis, taken here as 0.20. Then Mander’s stress-strain equation for confined concrete [8] is used in conjunction with the current confining stress to determine the axial compressive stress for the given strain (Fig. 4) at all slices of the critical section. Figure 4 gives multiple compressive stress-strain results generated for different constant confining levels based on Mander’s stress-strain equation for confined concrete [8]. The confined stress-strain path for a slice of the cross-section that has increasing confinement from GFRP, as the axial strains get larger, is guided by these constant-confinement lines, crossing over them one after another, as shown by the black arrow line in Fig. 4 for the extreme compression edge of the confined core of Column 2. In reality, there are an infinite number of constant-confinement paths, all unique and not crossing over each other. The final point of the path with increasing confining pressure intersects the curve with constant confining stress of 1788 psi (12.3 MPa) at the axial stress and strain for the element at failure, consistent with hoop strain and stress failure for Column 2. At this point, the program ANDRIANNA [9] finds the compressive axial strain, then the hoop strain. From the material properties of the hoop material (linear or nonlinear) and the hoop strain, the hoop stress is determined, allowing the current confining pressure to be calculated. Based on Mohr’s circle, the compressive stress is the same on all sides of a stress element (Fig. 4b), for any angle considered. Finally, with the confining pressure of 1788 psi (12.3 MPa) at the given axial strain, the axial stress from the constant-confinement curve is determined, which is the same axial stress for the changing confinement response of Column 2 shown in Fig. 4.

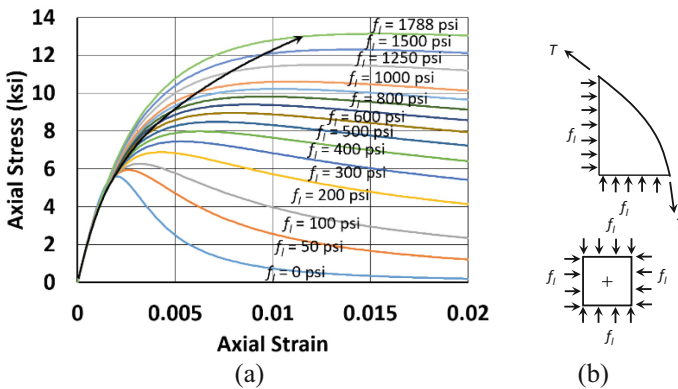


Fig. 4. Incremental confinement model for concrete: (a) compressive stress-strain path (GFRP, Column 2) and (b) force equilibrium and stress element (1 ksi = 6.895 MPa)

The confining pressure $f_l = 0.5 \rho_h \sigma_h$ is derived from statics of a small arc length of the transverse rebar over one slice width and is a function of the percentage of transverse steel and current hoop stress at a given slice. The current Poisson’s ratio $\mu_t = \mu_e + (e \sigma_1') / (2 f_l)$, adds a term divided by the current confining pressure to the initial elastic value; as the confining stress approaches zero the expansion rate increases without bound, indicating the observed instability and failure of unconfined concrete under large strains. The term $e = (1 + (\eta \epsilon_1 + J)^{-1})^{-1}$ in Poisson’s ratio μ_t is an efficiency factor for energy

transfer from concrete axial strain to hoop strain. From Mander's original tests on axially loaded columns [8] it was found that the values of $h = 20$ and $J = 1/3$ agreed best with the results [10, 11], providing more efficient energy transfer with larger strains.

Force-displacement and moment-curvature analysis results are given in Fig. 5 for all the columns considered. While the ultimate force for all the columns is similar, as designed, there is a large difference in deformation capacities, with the largest displacements and curvatures for the all-steel reinforced Column 1. Although Columns 2 and 3 have the same primary vertical steel as Column 1, their displacement capacity is limited due to the GFRP transverse reinforcing bar which has much less hoop strain capacity than steel reinforcing bar.

The increase in lateral force at a given displacement for Columns 2 and 3 over Column 1 (Fig. 5a) is due to higher confining stresses from the transverse GFRP reinforcing bar for these columns, which causes larger axial compressive stresses for a given strain at the critical section and, hence, increased moment for a given curvature (Fig. 5b). Reduced hoop strain capacity of GFRP compared to steel is responsible for ultimate displacements and curvatures for Columns 2 and 3 to be less than one-half of the values from Column 1, which has steel transverse reinforcement. Regardless, Columns 2 and 3 still have relatively good predicted deformation and ductility capacities due to their vertical steel reinforcement at the critical section.

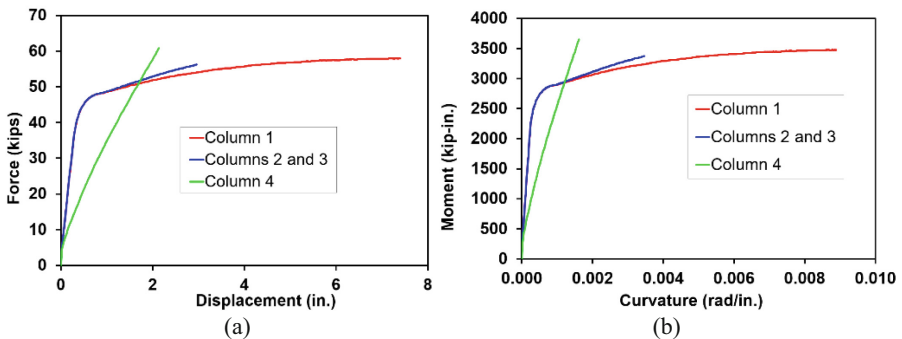


Fig. 5. (a) Force-displacement and (b) moment-curvature analysis results for all four columns (1 in. = 2.54 cm, 1 kip = 4.448 kN)

As expected, Column 4 with all-GFRP for vertical and transverse reinforcement, has the most limited deformation capacities in terms of curvatures and displacements (Fig. 5a), with about two-thirds the displacement values of Columns 2 and 3, and approximately one-quarter the displacement capacity of Column 1. Such limited deformation capacities make RC bridge columns with all GFRP reinforcement questionable for seismic design, although the combination of vertical steel and transverse GFRP reinforcement shows promise, as does all GFRP in addition to steel starter bars, so long as displacement capacities exceed earthquake demands.

Stress-strain results for the extreme tension and compression bars, at the critical section, for all four columns are given in Fig. 6. It is clear from Fig. 6 that while the columns with steel followed their idealized stress-strain behavior to large strains, Column 4 followed the linear-elastic behavior of GFRP. Similarly, concrete compression stress-strain responses show the difference between the constant confinement stresses of Column 1 (constant once the transverse steel yields early in the loading) with the changing confining stresses of the other columns due to the transverse GFRP rebar (Fig. 7), with Columns 2 and 3 reaching an impressive compressive stress of about 13 ksi (89.6 MPa), which is more than double the unconfined concrete strength. Incremental confinement was used for all four column analyses, including Column 1 which was all steel rebar. In all cases the ultimate compressive strain capacity of the concrete was based on failure of the transverse reinforcement, which suddenly makes the confined core unconfined, leading to complete failure of the columns and bridge structure, unable to support the dead load of the bridge at these large compressive strains.

Results in Fig. 7b show that failure of all four columns is due to hoop fracture, with ultimate steel strain capacity of 0.12 resulting in Column 1 failure while the 0.019 strain capacity of GFRP limited the behavior of Columns 2, 3 and 4. The effect from increasing

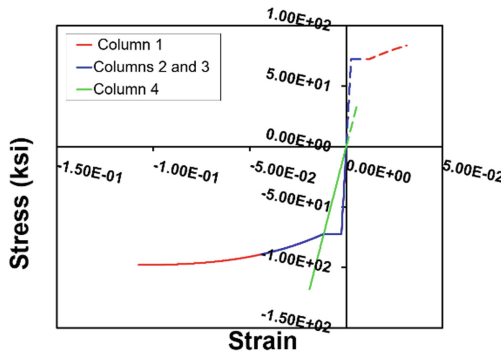


Fig. 6. Tension and compression stress-strain responses for extreme rebars, all columns (1 ksi = 6.895 MPa)

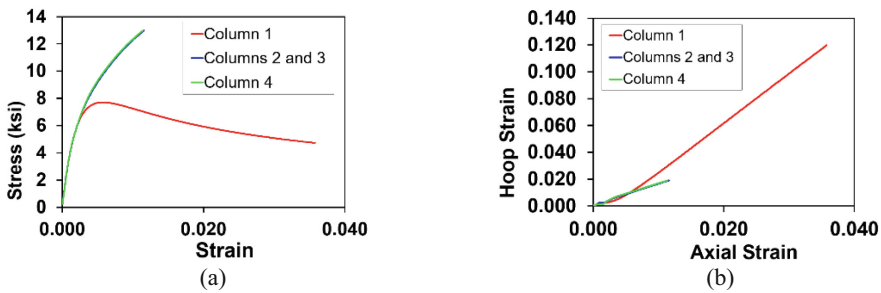


Fig. 7. (a) Concrete compression stress-strain responses at extreme fiber and (b) hoop strain versus axial strain of extreme compression fiber for all four columns (1 ksi = 6.895 MPa)

confining pressure from transverse GFRP, with loading, on limiting concrete expansion is clear from the changing Poisson's ratio given in Fig. 8a, as well as the confining pressures in Fig. 8b. Note how the confining pressure for Column 1 initially increases until the transverse steel rebar yields early in the analysis, and then remains constant from then on, whereas the confining pressure continues to increase for Columns 2, 3 and 4 due to the transverse GFRP rebar which remains linear-elastic until failure.

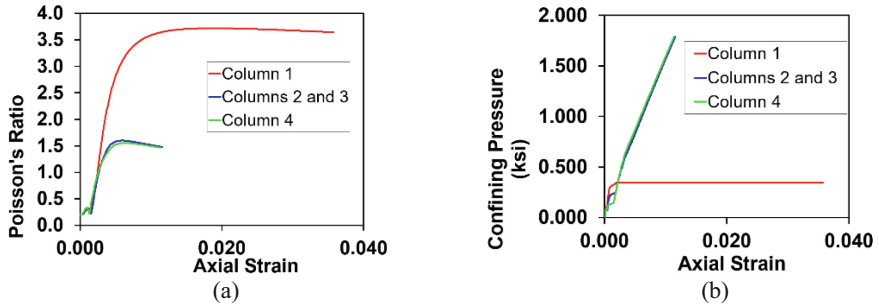


Fig. 8. (a) Poisson's ratio versus axial strain of extreme compression fiber and (b) confining pressure versus axial strain of extreme compression fiber, all columns (1 ksi = 6.895 MPa)

5 Conclusions

Analyses of four RC bridge columns showed that replacing traditional steel rebar with GFRP rebar reduces the displacement capacity while providing similar force capacity. When the vertical reinforcement is steel and transverse reinforcement is GFRP, the displacement capacity is less than one-half of the all-steel column, and when both transverse and vertical rebar are GFRP the displacement capacity reduces further to approximately one-quarter of the all-steel column, resulting in a brittle behavior of the RC element. In all four cases, the columns failed when the hoop strains reached the strain capacity of the material, with steel failure for Column 1, and GFRP failure for Columns 2, 3 and 4. The worst performing column, in terms of displacements, is Column 4 which has GFRP for both vertical and transverse bars, significantly restricting the displacements. Columns 2 and 3 have the same behavior since they both have GFRP for transverse reinforcement and vertical steel reinforcement that crosses the critical column-footing interface, with Column 3 achieving this by added steel starter bars while Column 2 has vertical steel reinforcement for the full column height, and into the footing. Since earthquake design requires displacement capacity to be greater than displacement demand, the results show that using GFRP for both transverse and vertical reinforcement (Column 4) is not realistic in high seismic zones due to the severely limited displacement capacity compared to a typical column with steel reinforcement (Column 1). However, when steel starter bars are used to cross the column-footing interface (Column 3), then the remainder of the vertical rebar up the column height can be GFRP and the transverse rebar can also be GFRP, resulting in performance that may be satisfactory in many instances.

ANDRIANNA [9] was modified for the analysis of the four columns considered, allowing an incremental concrete confinement approach based on energy principles [10, 11] and the Mander model [8]. When transverse reinforcement is GFRP, an incremental confinement analysis is necessary due to the linear-elastic behavior of GFRP until failure. As the axial compressive strains increase due to bending, the concrete expands into the confining reinforcement, developing hoop strains, hoop stresses, and confining stresses to the core concrete that change and get larger as the analysis continues. Furthermore, for a given axial strain the axial stress increases with larger confining pressure. The other advantage to the incremental confinement approach is that hoop strains and stresses are monitored throughout the analysis, allowing column failure to be directly determined. This is very different than the standard Mander model [8] where the ultimate compressive strain capacity is found before the lateral analysis, assuming constant confining stress.

References

1. Priestley MJN, Seible F, Calvi GM (1996) Seismic design and retrofit of bridges. John Wiley and Sons, New York
2. Dowell RK (2023) Reconnaissance report of observed structural bridge damage. Mw 7.8 Turkey earthquake of 2023. Structural Engineering Research Project SERP- 23/03
3. Afifi MZ, Mohamed HM, Benmokrane B (2014) Axial capacity of circular concrete columns reinforced with GFRP bars and spirals. *J Compos Constr* 18(1):04013017
4. Prajapati GN, Farghaly AS, Benmokrane B (2022) Behavior of reinforced concrete columns with hybrid reinforcement (steel/glass fiber-reinforced polymer) under reversed cyclic load. *ACI Struct J* 119(4)
5. De Luca A, Matta F, Nanni A (2010) Behavior of full-scale glass fiber-reinforced polymer reinforced concrete columns under axial load. *ACI Struct J* 107(5):589
6. Elshamandy MG, Farghaly AS, Benmokrane B (2018) Experimental behavior of glass fiber-reinforced polymer-reinforced concrete columns under lateral cyclic load. *ACI Struct J* 115(2):337–349
7. Ali MA, El-Salakawy E (2016) Seismic performance of GFRP-reinforced concrete rectangular columns. *J Compos Constr* 20(3):04015074
8. Mander JB (1983) Seismic design of bridge piers. Ph.D. Dissertation, University of Canterbury, Christchurch
9. Dowell RK (1999) ANDRIANNA user's manual, version 1
10. Hose YD, Brestel D, Seible F, Dowell, RK (2000) Assessment of hoop strains in the flexural plastic hinge region of typical bridge columns. UCSD report no. SSRP-2000/11, p 119
11. Dowell RK, Seible F (2001) Incremental confinement effects in a moment-curvature analysis. In: Proceedings 6th caltrans seismic research workshop, Sacramento